Theoretical studies on absorption, emission, and resonance Raman spectra of Coumarin 343 isomers

Wenpeng Wu, Zexing Cao, and Yi Zhao

Citation: J. Chem. Phys. **136**, 114305 (2012); doi: 10.1063/1.3693264
View online: http://dx.doi.org/10.1063/1.3693264
View Table of Contents: http://jcp.aip.org/resource/1/JCPSA6/v136/i11
Published by the American Institute of Physics.

Theoretical studies on absorption, emission, and resonance Raman spectra of Coumarin 343 isomers

Wenpeng Wu, Zexing Cao, and Yi Zhao[a)]
State Key Laboratory for Physical Chemistry of Solid Surfaces and Fujian Provincial Key Lab of Theoretical and Computational Chemistry, College of Chemistry and Chemical Engineering, Xiamen University, Xiamen 361005, People's Republic of China

(Received 15 December 2011; accepted 20 February 2012; published online 15 March 2012)

The vibrationally resolved spectral method and quantum chemical calculations are employed to reveal the structural and spectral properties of Coumarin 343 (C343), an ideal candidate for organic dye photosensitizers, in vacuum and solution. The results manifest that the ground-state energies are dominantly determined by different placements of hydrogen atom in carboxylic group of C343 conformations. Compared to those in vacuum, the electronic absorption spectra in methanol solvent show a hyperchromic property together with the redshift and blueshift for the neutral C343 isomers and their deprotonated anions, respectively. From the absorption, emission, and resonance Raman spectra, it is found that the maximal absorption and emission come from low-frequency modes whereas the high-frequency modes have high Raman activities. The detailed spectra are further analyzed for the identification of the conformers and understanding the potential charge transfer mechanism in their photovoltaic applications. © *2012 American Institute of Physics*. [http://dx.doi.org/10.1063/1.3693264]

I. INTRODUCTION

In recent years, organic solar energy cells have attracted much attention as a kind of renewable energy sources. Organic dye-sensitized solar cell (DSSC) among them is becoming popular with the properties of cheapness and relatively high efficiency.[1–3] In DSSC, organic dye molecules play a key role since they determine both the efficiencies of photo absorption and charge injection into semiconductors. The 7-amino coumarin dye molecules (such as Coumarin 1, Coumarin 6, Coumarin 120, and Coumarin 343) have strong absorption and emission in the blue and green regions of the spectra.[4,5] They thus become ideal candidates as dye photosensitizers.[6–11] In addition, these dye molecules have other applications in laser dyes,[4,5] solvation and fluorescence probe molecules.[12–22]

Coumarin 343 (C343, see Fig. 1) is one of 7-amino coumarins and has been already used in DSSC.[7,9–11] It has a rigid julolidine structure and was first reported in 1975 with a high quantum yield of fluorescence in ethanol.[4] Its crystal was first prepared from a chloroform solution by slow evaporation in 1996.[23] The detailed structural investigations show that the carboxylic group is coplanar with the planar coumarin moiety, the two piperidine rings take flattened sofa conformations and there is an intramolecular hydrogen bond (H-bond) between the carbonyl group (–C=O) and carboxylic group (–COOH). Meanwhile, experimental measurements show that the absorption and emission spectra of C343 strongly depend on the solvent polarity, the H-bond donation and acceptance abilities.[5,14,15,24–29] Especially, the different pH values of the solution may significantly change spectral properties.[12,21,28,30,31] For instance, C343 in basic solution may be ionized by one proton and become a deprotonated anion whose spectra are definitely different from the neutral C343.

Available experimental studies have supplied the fundamental spectra information of C343 for the construction of DSSC. However, C343 essentially has many different conformations, and it is not still fully understood how different geometries affect their spectral properties. In this paper, therefore, we focus on this problem theoretically. In the past decades, in fact, stable ground states and pure electronic absorption spectra of coumarin derivatives in gas phase and in solution have been studied by using quantum chemical methods.[32–43] For instance, in the framework of density functional theory (DFT), Preat *et al.*[33] investigated the UV electronic absorption spectra of substituted coumarins with various basis sets and functionals. It turns out that the Becke-Lee-Yang-Parr functional (B3LYP) together with the polarized continuum model (PCM) provides valid ground-state geometries and the consistent UV spectra with experimental measurements. Cave *et al.*[32] explored various properties of C152, C153, C102, and C343 with DFT and time-dependent density functional theory (TDDFT) in gas phase. Their calculations reveal that the syn conformer is more stable than the anti conformer by 0.011 eV according to the calculations on C153 and TDDFT is an accurate and good tool for the examination of the ground and excited states of coumarins. For C343, several theoretical investigations[35,39,41,43] have been also done. However, these studies mainly involve only one conformer, one excited state, and the solvent effect is not considered. To fully understand the photo-absorption of C343 conformers in a wide energy regime and in different environments, we investigate the geometries, ionization energies, and pure electronic absorption spectra in both gas phase and solution.

[a)]Author to whom correspondence should be addressed. Electronic mail: yizhao@xmu.edu.cn.

On the other hand, photo absorption and emission are intrinsically involved in the effect of the nuclear motions of molecules. The single-point excitation energies cannot reveal the detailed spectral property although they indeed predict the position of spectral peaks under Franck-Condon approximation. Therefore, vibrationally resolved spectra are essential to straightforwardly compare with experimental data and find the mode-specific effect on the spectra. Especially, resonance Raman spectroscopy can determine the mode-specific reorganizations and corresponding mode frequencies. An analysis of the resonance Raman spectra intensities can also obtain the excited state dynamics, which is particularly useful to describe the photo-induced ultrafast charge transfer process. Another purpose of the present paper is therefore to predict these vibrationally resolved spectra.

Compared to the pure electronic absorption and fluorescence, vibrationally resolved spectra need both quantum chemical calculations and quantum dynamical simulations. In the dynamical simulations, we use correlation function method in the time-domain to incorporate the vibrational motions. In the harmonic approximation, the analytical formulas for the correlation functions are available.[44–46] To get the vibrational modes on the ground and excited states, the project techniques[47] are employed in which Dushinsky rotational matrix can also be obtained. With the use of these methods, we aim to investigate the mode-specific contribution to the spectra in C343 conformers, which may be helpful to succeedingly design the high efficient DSSC.

The paper is organized as follows. Section II outlines the spectral theory and quantum chemical methods used in the paper. Section III illustrates results including the geometries, the ionization potentials, the pure electronic absorption spectra, vibrationally resolved electronic absorption, fluorescence spectra, and resonance Raman spectra. Concluding remarks are given in Sec. IV.

II. COMPUTATIONAL METHODS

A. Computational method for vibrationally resolved spectra

Vibrationally resolved spectra generally involve in the first excited state and ground state of molecules. For such two-state molecules, the Hamiltonian is given by

$$H = |g\rangle H_g \langle g| + |e\rangle (H_e + \omega_{eg} - i\gamma)\langle e|. \tag{1}$$

Here, $|g\rangle$ and $|e\rangle$ represent the electronic ground and excited states, respectively. ω_{eg} is the difference between the potential energy minima of the two electronic states. γ is the factor related to the $|e\rangle$-state lifetime. Under the harmonic oscillator approximation, the nuclear Hamiltonians of the electronic ground and excited states can be written as

$$H_g = \frac{1}{2}\sum_j^N \omega_{g_j}\left(P_{g_j}^2 + Q_{g_j}^2\right), \tag{2}$$

$$H_e = \frac{1}{2}\sum_j^N \omega_{e_j}\left(P_{e_j}^2 + Q_{e_j}^2\right). \tag{3}$$

Here, P and Q are the dimensionless momentum and nuclear coordinates. ω is the vibrational frequency. Usually, the normal-mode coordinates of ground and excited states are different, and they can be correlated by Duschinsky rotation matrix S by $Q^e = SQ^g + D$. D is the displacement between the equilibrium configurations of the two electronic states. The corresponding eigenstate equation is written as

$$H_i|n_i\rangle = \hbar\epsilon_{n_i}|n_i\rangle, \tag{4}$$

where ϵ_{n_i} and $|n_i\rangle$ stand for the nth vibrational eigenvalue and eigenwavefuction in the ith electronic state, respectively.

The optical excitation taken place in the molecule is described by a dipole operator

$$\mu = |e\rangle\mu_{eg}\langle g| + |g\rangle\mu_{ge}\langle e|, \tag{5}$$

where μ_{eg} is the molecular transition dipole moment. The vibrationally resolved absorption cross section $\alpha(\omega)$ and emission cross section $\beta(\omega)$ are calculated by

$$\alpha(\omega) \propto \omega \int_{-\infty}^{\infty} dt\ e^{i(\omega-\omega_{eg}+\epsilon_{n_g})t-\gamma|t|}C_a(t), \tag{6}$$

$$\beta(\omega) \propto \omega^3 \int_{-\infty}^{\infty} dt\ e^{-i(\omega-\omega_{eg}+\epsilon_{n_e})t-\gamma|t|}C_e(t) \tag{7}$$

with the dipole-dipole auto-correlation function

$$C_a(t) = \sum_m P_{m_g}\langle g, m_g|\mu e^{-iH_e t}\mu|g, m_g\rangle, \tag{8}$$

$$C_e(t) = \sum_m P_{m_e}\langle e, m_e|\mu e^{-iH_g t}\mu|e, m_e\rangle, \tag{9}$$

where P_{m_i} is the thermal population of the mth vibrational state in the ith electronic state. For the resonance Raman spectra (RRS), the differential photon scattering cross section can be expressed as[48]

$$\sigma(\omega_L, \omega_S) = \frac{4\omega_L\omega_S^3}{9c^4}S(\omega_L, \omega_S), \tag{10}$$

where ω_L and ω_S denote the frequencies of the incident and scattering photons, respectively, c is the speed of the light, and the resonance Raman line shape $S(\omega_L, \omega_S)$ is given by the Kramers-Heisenberg-Dirac expression[49]

$$S(\omega_L, \omega_S) = \sum_{n_g, m_g} P_{n_g} I_{n_g, m_g}(\omega_L)\delta(\omega_S - \omega_L - \epsilon_{n_g} + \epsilon_{m_g}), \tag{11}$$

where I_{n_g,m_g} is the Raman excitation profile for the transition from the vibrational state $|n_g\rangle$ to $|m_g\rangle$. In the time domain, it has a form

$$I_{n_g,m_g} = 2\pi\left|\int_0^{\infty} dt e^{i(\omega_L-\omega_{eg}+\epsilon_{n_g})t-\gamma t} \times C_{mn}(t)\right|^2 \tag{12}$$

with the correlation function

$$C_{mn}(t) = \langle g, m_g|\mu e^{-iH_e t}\mu|g, n_g\rangle. \tag{13}$$

It is clear now that both the absorption (emission) and Raman spectra can be calculated by the time-dependent correlation function $C_{mn}(t)$. When compared Eq. (8) and Eq. (9) with Eq. (13), both incorporate the excited-state dynamics. The only difference is that in the absorption, the excited-state

propagation is projected back to the initial vibrational state in the electronic ground state, whereas it is projected to different vibrational state in RRS. The key step for the calculations of the spectra, therefore, is to propagate the excited-state wavefunction. There are considerable approaches to do it.[50–53] Under Condon approximation, these correlation functions have analytical solutions.[44] Thus, once the correlation functions are known, the absorption, fluorescence, and RRS can be obtained by simple Fourier transforms.

B. Quantum chemical calculation method

The geometries and the vibrational frequencies of the Coumarin 343 conformers at their ground states are determined by using the B3LYP functional[54–56] and the 6-31+G** basis set. The numerical simulations confirm that B3LYP/6-31+G** treatment exhibits a good balance between accuracy and computational cost (see Sec. III). Based on the optimized geometries of the ground states, the single point energies and the vertical ionization potentials are computed by the B3LYP/6-311++G(3df,2pd) method. In order to get the adiabatic ionization potentials, the geometries of the ground-state cations are optimized at the UB3LYP/6-31+G** level of theory. The vertical excitation energies are obtained by TD-B3LYP[57–61] /6-31+G**, which is also used to optimize the geometry of the first excited state.[62,63] Meanwhile, the frequency analysis is performed to assess their stability and obtain the normal modes. The solvent effect of methanol (MeOH) is incorporated by using the conductive polarized continuum model (CPCM).[64,65] All the frequencies are scaled by a factor of 0.9642 (Ref. 66) and the quantum chemical calculations are performed with GAUSSIAN 09 programme package.[67]

To get the shifts of the normal-mode coordinates in the electronic ground and excited states, one may start from the relationship between the Cartesian coordinates of the optimized donor and acceptor states by

$$q_a = q_d + \Delta q, \tag{14}$$

where q_d and q_a represent the mass-weighted Cartesian coordinates of the donor and acceptor states, respectively, Δq is the corresponding shift. The normal mode coordinates Q can be transformed from Cartesian coordinates q as[47]

$$Q = Lq, \tag{15}$$

where L is the transform matrix. It can be obtained from the diagonalization of the Hessian matrix K by

$$L^T K L = \omega^2, \tag{16}$$

where ω are the frequencies. By using Eq. (15), Eq. (14) can be cast into

$$Q_a = L_a L_d^T Q_d + L_a \Delta q, \tag{17}$$

where L_d and L_a correspond to the transform matrix for the donor and acceptor states, respectively, and $L_a L_d^T (= S)$ is called Duschinsky rotation matrix, which is approximated to unit in calculation. ΔQ is thus obtained from $L_a \Delta q$.[47]

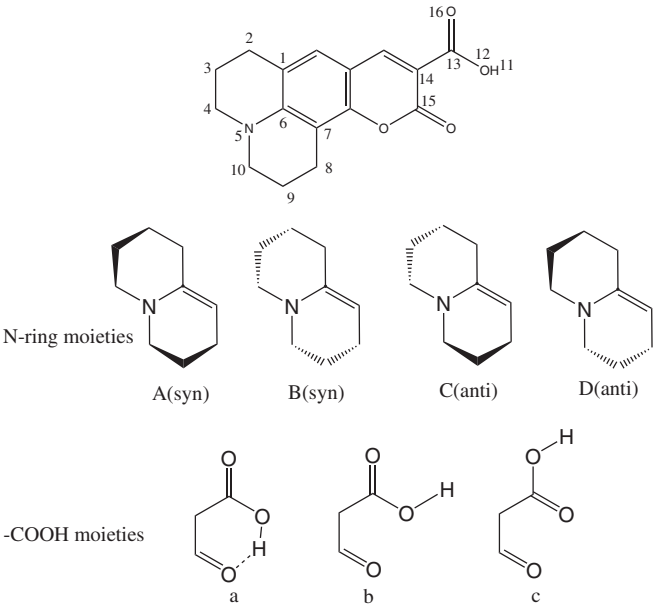

FIG. 1. Structures of building components of C343.

III. RESULTS AND DISCUSSION

A. Geometries and stability

1. Geometries of the ground state

According to the previous studies on C343,[32] we choose four N-ring moieties (abbreviated as A, B, C, and D) and three carboxylic group (–COOH) moieties (abbreviated as a, b, and c), as depicted in Fig. 1. A, B and C, D correspond to the syn and anti structures, respectively. These basic building components can construct 12 different isomers of C343, such as Aa, Ba, Cb, Dc, and so on.

In order to select the appropriate quantum chemical method and basis set, we take the Ca isomer as the test system, because Ca with the intramolecular H-bond can provide a direct comparison with experimental measurement.[23] First, we use different methods with the same basis set 6-31G**, including HF, MP2, and DFT with the functionals PBE0, BLYP, B3LYP, B3PW91, CAM-B3LYP, and ω-B97XD. From the obtained ground-state geometries and the available crystal structure data,[23] we calculate the correlation coefficient (R) and standard deviation (SD). The R and SD are obtained by using linear fitting of the bond lengths between non-hydrogen atoms. The results are listed in Table S1 of the supplementary material.[68] We note that B3LYP calculations exhibit the best performance with R = 0.9925 and SD = 0.0108. Second, we test different basis sets, including 6-31G**, 6-31+G**, 6-31++G**, 6-311G**, 6-311+G**, 6-311++G**, and 6-311++G(3df,2pd) (Table S2 in Ref. 68). It is found that the 6-31+G** basis set shows a good balance between accuracy and computational cost (R = 0.9936 and SD = 0.0099). Accordingly, the B3LYP/6-31+G** approach is employed in the geometry optimization.

With the adopted basis set and method, we optimize the ground states of 12 isomers in both vacuum and methanol solution. We note that the optimized geometries in both the vacuum and solution are quite similar, where the nitrogen atom

TABLE I. Selected dihedral angles of different conformers of C343 (in degree).

Dihedral angle	Aa	Ba	Ca	Da	Expt.[a]
5-4-3-2	57.2(55.5)[b]	−57.0(−55.0)	−50.3(−50.6)	50.2(50.5)	−51.5
5-10-9-8	−57.8(−56.7)	57.8(56.8)	−52.3(−52.3)	52.3(52.4)	−49.8
4-5-6-1	8.9(4.9)	−8.2(−3.8)	6.9(5.8)	−7.1(−5.9)	6.6
10-5-6-7	−11.6(−8.1)	12.0(8.9)	4.0(3.9)	−3.8(−3.8)	8.1
Dihedral angle	Ca	Cb	Cc		
11-12-13-14	0.0(0.1)	180.0(180.0)	180.0(180.0)		
11-12-13-16	180.0(180.0)	0.0(0.0)	0.0(0.0)		
16-13-14-15	180.0(180.0)	−179.9(−179.8)	−0.1(−0.4)		

[a]Experimental data from Ref. 23.
[b]The values outside the parentheses are for the gas phase and the numbers in parentheses are for the MeOH solution.

and the –COOH group are nearly coplanar with the coumarin moiety, and the carbon atoms 4 and 10 slightly deviate from the plane of coumarin moiety while the atoms 3 and 9 show notable deviation.

Selected dihedral angles are compiled into Table I. As Table I shows, the Ca structure among 12 isomers is in better agreement with the experimental measurement.[23]

Table II displays the relative ground-state energies of different isomers. Clearly, the relative energies are nearly independent of the N-ring conformers (A, B, C, and D), and they are basically determined by the –COOH conformers (a, b, and c). For instance, the energy differences among Aa, Ba, Ca, and Da isomers are within 0.01 eV, while the energies of the isomers without the intramolecular H-bond (conformer b) are about 0.25 eV higher than those with the H-bond (conformer a). In vacuum, the energies of isomers containing the c moiety are generally 0.05 eV higher than those with the b subunit, but their energy differences almost vanish in methanol solution. This suggests that the isomers with the b or c moiety may coexist equally from the thermodynamical point of view. Furthermore, the most stable structure Aa (syn-form) in the gas phase is slightly higher in energy than the lowest-energy species Ca (anti-form) by 0.003 eV in methanol solution. The predicted bond lengths of Ca in solution show better agreement with experiment (R = 0.9972 and SD = 0.0064) among the isomers, which lends further support to that the Ca isomer most probably corresponds to the experimental structure.[23]

2. Ionization potentials

As an electron donor, the ionization energy is an important parameter to characterize the electron-donating ability. We calculate the vertical ionization potentials (VIPs) and adiabatic ionization potentials (AIPs) of different C343 isomers. The results are listed in Table III.

TABLE II. Relative energies of different conformers of C343 (in eV).

	A	B	C	D
a	0.000(0.003)[a]	0.002(0.007)	0.010(0.000)	0.010(0.001)
b	0.255(0.257)	0.257(0.260)	0.266(0.255)	0.266(0.256)
c	0.312(0.257)	0.314(0.259)	0.322(0.254)	0.319(0.252)

[a]The values outside the parentheses are for the gas phase and the numbers in parentheses are for the MeOH solution.

As expected, AIPs are slightly smaller than the corresponding VIPs. The predicted values are close to the previously available data of 7.36 eV (VIP of syn-C343 in vacuum) and 7.23 eV (AIP of syn-C343 in vacuum).[32] It can also be seen from Table III that IPs of the structures with the intramolecular H-bond are higher than those without, and IPs for the syn-conformers are larger than the corresponding anti-conformers. Furthermore, the energy difference between VIPs and AIPs for syn-conformers are larger than those for the anti-conformers, suggesting that the structural relaxation of the syn-form cations is slightly more remarkable than the anti-form cations, compared to their neutral counterparts.

Taking into account of the ionization energies, one can estimate coarsely that the anti C343 conformer without the intramolecular H-bond in DSSC is slightly easier to inject electrons to the conduction band of semiconductor than others. Structurally, the adsorption of such anti-form isomers on the oxide surface is more facile and effective than those with the intramolecular H-bond. As shown in Table III, in methanol solvent, the VIPs are reduced by about 1.6–1.8 eV, showing remarkable solvation effect. Presumably, the presence of methanol solvent may facilitate the electron injection, compared to the gas phase.

B. Spectroscopic properties

1. Pure electronic absorption spectra

It is known that the pure electronic absorptions correspond to the vertical electronic excitations from the optimized ground-state geometries. We calculate these energies up to the 20th excited state. Before calculating the excitation

TABLE III. Ionization potentials of different conformers of C343 (in eV).

Species	VIP	AIP	Species	VIP	AIP
Aa	7.409(5.624)[a]	7.262(5.516)	Ca	7.345(5.594)	7.232(5.497)
Ab	7.203(5.548)	7.056(5.439)	Cb	7.136(5.516)	7.027(5.421)
Ac	7.217(5.552)	7.058(5.440)	Cc	7.150(5.520)	7.030(5.424)
Ba	7.407(5.622)		Da	7.345(5.594)	
Bb	7.200(5.547)		Db	7.136(5.516)	
Bc	7.215(5.551)		Dc	7.151(5.520)	

[a]The values outside the parentheses are for the gas phase and the data in MeOH are given in parentheses.

energies, we first test the accuracy of the basis set. It is found that B3LYP calculations with the 6-311++G(3df,2pd) and 6-31+G(d,p) basis sets predict very similar excitation energies. For example, the predicted first vertical excitation energy difference for Aa isomer from both basis sets is only 0.01 eV. Therefore, the relatively small 6-31+G(d,p) basis set is used in succeeding calculations. Compared to the previous calculation[32] by the PBE0 functional with the 6-311G(d,p) basis set in vacuum, the present value for the Aa isomer is lower than that by 0.15 eV. The available observed values of the maximum absorption wavelength (λ_{max}) of C343 varies from different literatures, including 430 nm,[41] 437.5 nm,[15] 442 nm,[7] 445 nm,[12] 446 nm[69] in MeOH solvent. Our calculations reveal that λ_{max} of different neutral isomers are in the range of 428–435 nm (see details in Table S3 in Ref. 68), in good consistence with the experimental values.

In neutral C343 molecules, the carboxylic group can be dissociated into the carboxylate anion and the proton under the certain condition, such as surface adsorption on the oxide semiconductor. Although the hydrogen atom of the carboxylic group in "a", "b", and "c" conformers has different circumstances, their deprotonated anions are the same. Herein we also optimized the geometries of the anionic Aa and Ca conformers (abbreviated as Aa-a and Ca-a) and calculated their vibrational frequencies. Compared to the neutral form, the carboxylate group is not coplanar with the coumarin moiety, and the torsion angle is about 70° in vacuum and 40° in MeOH, which will lead to different electronic transition properties. In MeOH solvent, λ_{max} of $S_0 \rightarrow S_1$ transition for Aa-a and Ca-a are 405.9 nm and 407.2 nm, respectively, in good agreement with the experimental value of 410 nm.[12]

Fig. 2 displays the simulated pure electronic absorption spectra of A and C conformers of C343 as well as their deprotonated anions Aa-a and Ca-a (Those of B and D conformers are exactly the same as the corresponding A and C conformers, which are shown in Fig. S1 in the supplementary material[68]).

In the simulations, the Lorentzian line-shape is used to fit the spectra, and the half-width at half height is 1500 cm^{-1}. It can be seen that the spectra of the neutral conformers are similar to each other, except for only slight position shift and intensity change. Based on calculations and orbital analysis of neutral C343, all of these spectral peaks arise from $\pi \rightarrow \pi^*$ transitions. $n \rightarrow \pi^*$ transitions are very weak with oscillator strengths about 0.0001, and they are buried in the near $\pi \rightarrow \pi^*$ transitions and difficult to be observed in the experiment. Due to lack of experimental electronic absorption spectra of C343 in both the gas phase and solution in 200–550 nm regime, we find some spectra of other coumarin derivatives, such as C153 (3-COOH is substituted by 4-CF_3)[4,22] and C314 (3-COOH is substituted by 3-$COOC_2H_5$),[4] whose absorption spectra above 200 nm have been determined experimentally. By comparing these experimental spectra[4,22] with neutral C343 spectra simulated here, one can easily find that their shapes are similar, indicating that our calculations are relatively reliable.

Compared to the spectra in vacuum, as shown in Fig. 2, the intensities of the $S_0 \rightarrow S_1$ absorptions in the solution become much stronger for both the anionic and neutral C343,

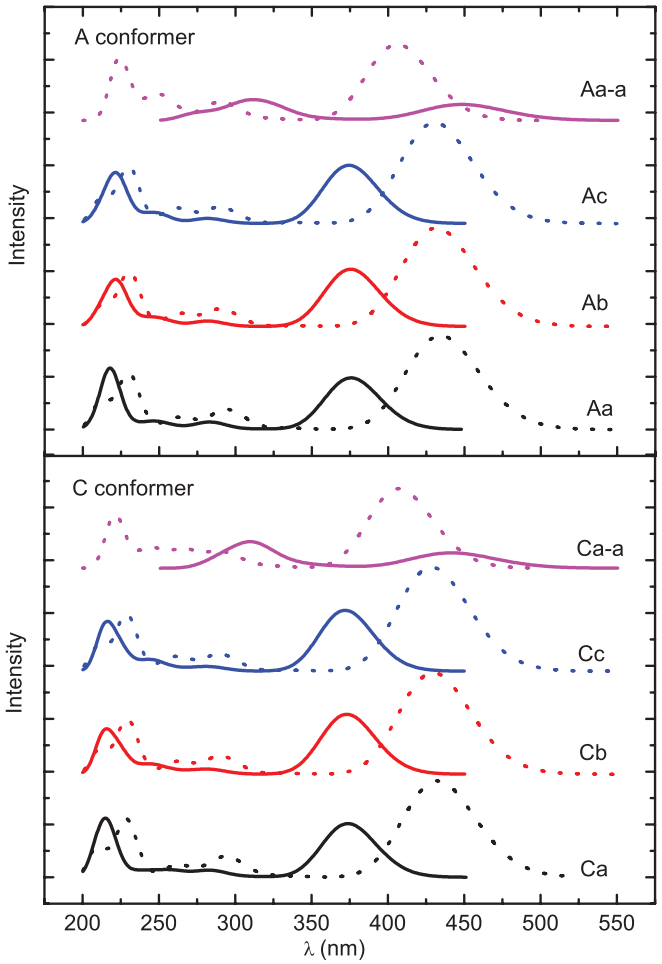

FIG. 2. Pure electronic absorption spectra in vacuum (solid lines) and in MeOH (dotted lines) of A and C conformers of C343.

however, the anionic and neutral spectra have blueshift and redshift, respectively. In order to get more insight into such similarity and difference, we calculate the dipole moments of the ground state (μ_{S_0}) and the first excited state (μ_{S_1}), as well as the corresponding transition dipole moments for the neutral and anionic C343 in vacuum. μ_{S_0} of Aa, Ca, Aa-a and Ca-a are 12.6, 13.0, 23.6, and 24.3 Debye, and μ_{S_1} are 16.6, 16.9, 12.7, and 10.2 Debye, respectively. For neutral form, $\mu_{S_0} < \mu_{S_1}$, while for anion form, $\mu_{S_0} > \mu_{S_1}$. As is known that for a polar molecule in polar solvent, such as MeOH, the bigger the dipole moment is, the stronger the interaction between the solute and the solvent is, and the more the energy decreases. Therefore in MeOH solvent, for the neutral form, the energy of the first excited state decreases more than the ground state, and the red shift occurs. The anion form shows the blue shift. The magnitude of transition dipole moments for Aa, Ca, Aa-a, and Ca-a are 2.58, 2.62, 1.32, and 1.27 a.u. in vacuum and 3.74, 3.78, 3.24, and 3.32 a.u. in MeOH solvent. It's obvious that those in MeOH are larger than those in vacuum, so the intensity increases in MeOH.

For further information of the pure electronic absorption spectra, we mark the exact position of each absorption peak in Figs. S2 and S3, and the assignments of these peaks are listed in Table S4 of the supplementary material.[68]

2. Vibrationally resolved electronic absorption and fluorescence spectra

To incorporate the effect of the vibrational motions on the spectra, we first calculate the normal-mode frequencies and shifts (Fig. S4 in Ref. 68) in the electronic ground and excited states. The spectra are then calculated from the time dependent correlation functions. It is already known that A and B isomers have very close pure electronic absorptions, and the same is true for C and D isomers. Therefore, we only focus on the A and C isomers. Fig. 3 displays the absorption and fluorescence spectra of A and C conformers at 298 K temperature in solution for the purpose of comparison with experiment.[12] In the simulations, the damping factor γ is 850 cm^{-1}. It should be noted that the simulated results are blue-shifted by 14 nm for the absorption and red-shifted by 17 nm for the fluorescence. These discrepancy of the maximal peaks comes from the energy gap of the excited and ground states for solvation effect beyond PCM model. The detailed comparison between simulation and experiment is listed in Table S5 of the supplementary material.[68]

However, the simulated spectral shapes are very well consistent with those of the experimental measurement except that the spectral peaks for different isomers have only a few nanometer shifts. Furthermore, the absorption and fluorescence have a nearly perfect mirror symmetry, manifesting that there are no large torsional motions between the ground and first-excited states.

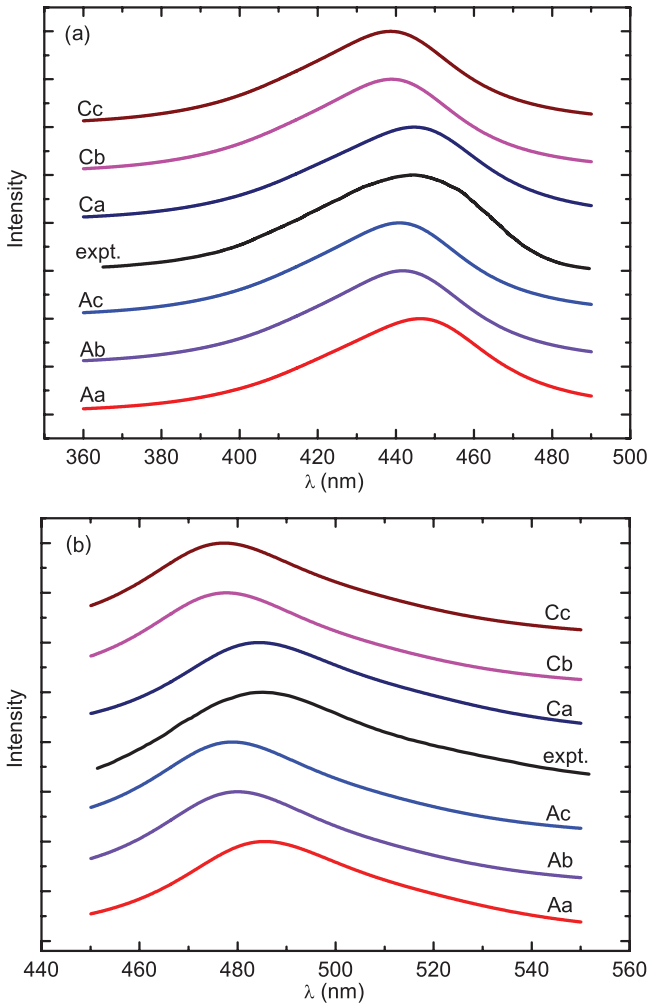

FIG. 3. (a) Vibrationally resolved electronic absorption and (b) fluorescence spectra of C343 in MeOH solution.

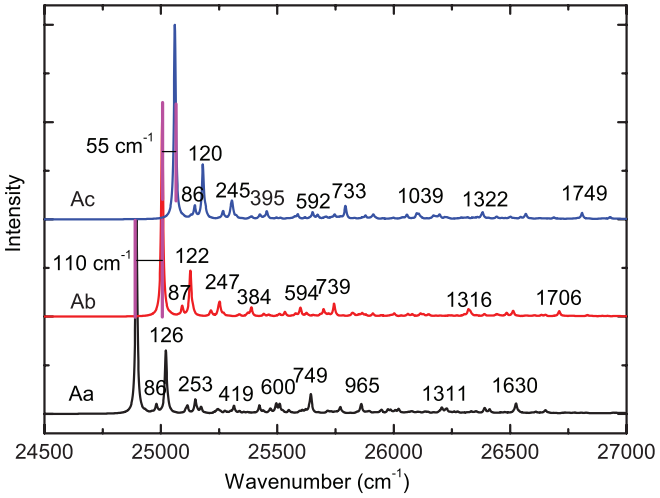

FIG. 4. Vibrationally resolved electronic absorption spectra of C343 with A conformation in gas phase at 0 K.

For a better understanding of the mode-specific absorption and fluorescence, we calculate the spectra in vacuum at 0 K and γ is 5 cm^{-1}. Figs. 4 and 5 display the absorption and fluorescence for A conformers, respectively (The spectra for other isomers are similar to A conformers, which are shown in Figs. S5– S8 in Ref. 68). It is found that the maximal absorptions and emissions correspond to 0-0 transitions for the three isomers although their origins are blue-shifted by 110 cm^{-1} for Ab and 165 cm^{-1} for Ac compared to Aa. The next maximal absorptions are the 0-1 transitions of the modes with 126 cm^{-1} for Aa, 122 cm^{-1} for Ab, and 120 cm^{-1} for Ac. The motions of these modes correspond to in plane bending vibrations of the whole molecules. For the modes with higher frequencies, the absorption strengths decrease explicitly. Their strengths are similar to 0–2 transitions of

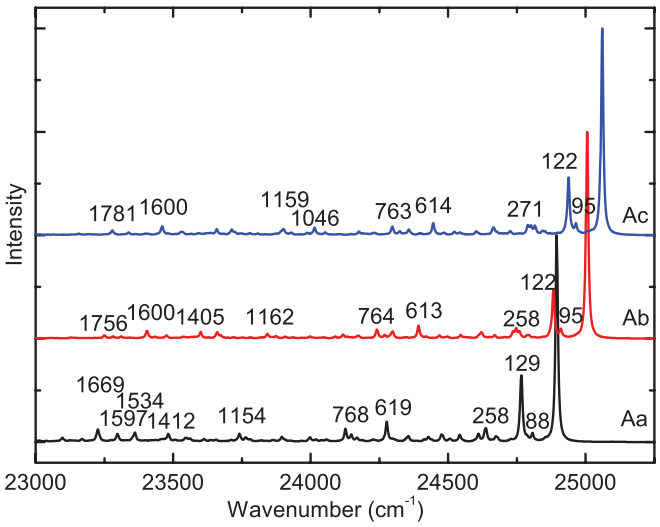

FIG. 5. Vibrationally resolved fluorescence spectra of C343 with A conformation in gas phase at 0 K.

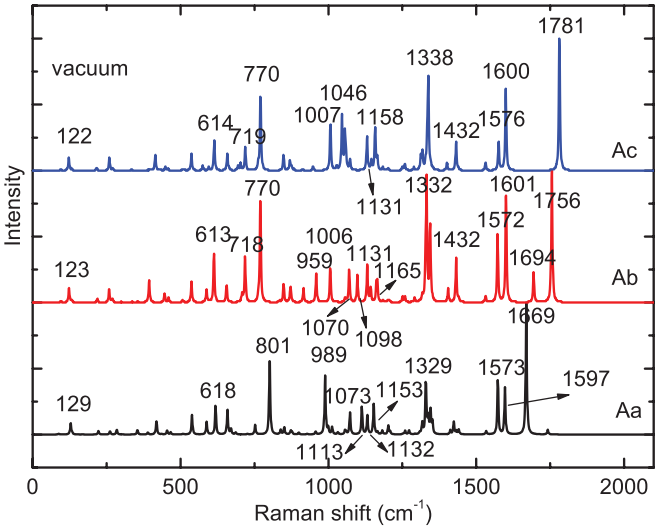

FIG. 6. Resonance Raman spectra of C343 with A conformation in gas phase at 298 K.

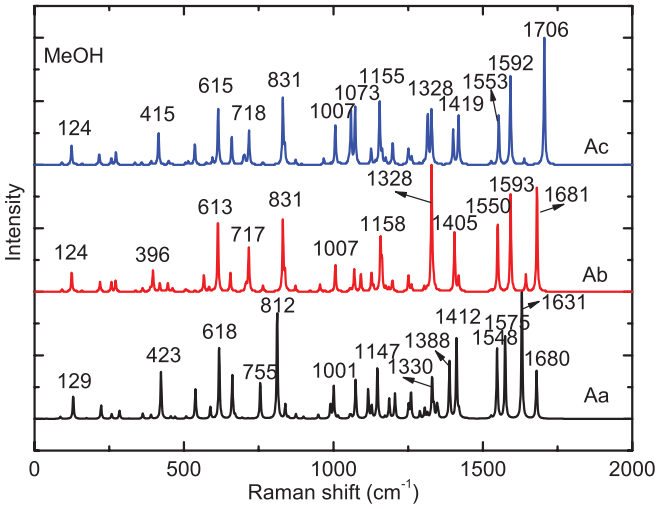

FIG. 7. Resonance Raman spectra of C343 with A conformation in MeOH solution at 298 K.

the modes with the frequencies of about 120 cm^{-1}. Although weak absorption strengths for high-frequency modes, the absorption peaks can still be observed. For instance, the absorption of 0–1 transition for the C=O stretching mode in the pyrone ring appears, and they are at 1630 cm^{-1}, 1706 cm^{-1}, and 1749 cm^{-1} for Aa, Ab, and Ac, respectively. However, their absorption strengths are similar, which suggests that the modes with and without intramolecular H-bond have a similar absorption property.

The fluorescence spectra (see Fig. 5) have a mirror symmetry compared to the absorption. But the frequencies of the modes are slightly larger than those for the absorptions. It is well known that the frequencies of the absorption and fluorescence correspond to those in the electronic excited and ground states, respectively. The quantum chemical calculations reveal that the mode frequencies in the ground state are larger than those in the excited state. These different mode frequencies are exactly described in the absorption and fluorescence.

3. Resonance Raman spectra

Similar to the vibrationally resolved absorption and fluorescence spectra, we calculate the RRS in vacuum. The results for A conformers are displayed in Fig. 6 and others are shown in Figs. S9– S12 in Ref. 68. The frequency range is limited to 0–2000 cm^{-1} because there are no resonance peaks between 2000 cm^{-1} and 2800 cm^{-1}, and only some very weak peaks appear above 2800 cm^{-1}. In the calculations, the excitation wavelength is chosen to be 508 nm on the basis of an experiment,[41] ω_{eg} is set at the same value used in the absorption spectra and temperature is 298 K. Experimentally, Savin's relation,[50,70,71]

$$I_i/I_j = \omega_i^3 D_i^2/\left(\omega_j^3 D_j^2\right) \tag{18}$$

is commonly used to determine the mode specific reorganization energies, where I_i is strength of RRS for the ith mode. The Savin's relation is obtained by the short time approximation in the Fourier transform (see Eq. (12)). To check the validity of this relation, we also calculate the RRS with the use of Eq. (18). It is found that the results (Figs. S13 in Ref. 68) are nearly the same as those shown in Fig. 6, manifesting that the short time approximation is valid for the present systems.

Fig. 6 explicitly shows that RRS are very similar for Aa, Ab, and Ac isomers, with weak peaks in low frequencies and strong peaks in high frequencies. However, for the same vibrational modes, the corresponding frequencies and RRS intensities are different. For example, C=O (in pyrone ring) stretching high-frequency vibrations occur at 1669 cm^{-1}, 1756 cm^{-1}, and 1781 cm^{-1}, for Aa, Ab, and Ac, respectively, similar to the vibrationally resolved fluorescence spectra except their intensities are much larger than those in the vibrationally resolved fluorescence spectra (Fig. 5). This property can be experimentally used to identify different isomers. In Aa isomer, the intensity of mode with CH_2 wagging and ring skeleton vibration motions (1329 cm^{-1}) is relatively weak, but they (1332 cm^{-1} in Ab and 1338 cm^{-1} in Ac) become very strong. This can be easily explained by the mode shifts in the excited states (Fig. S4 in Ref. 68) and Savin's relation (Eq. (18)). More interestingly, the intensity of mode with 801 cm^{-1} in Aa isomer are very similar to the modes with 770 cm^{-1} in Ab and Ac. However, they do not correspond to the same vibrational motions. The mode with 801 cm^{-1} corresponds to the out of plane bending of OH whereas the modes with 770 cm^{-1} are O=C–C–COOH out of plane bending vibration. These modes also can be easily used to determine the isomers with and without H-bond. The detailed assignment of each vibration mode is in Table S7 in Ref. 68.

Fig. 7 displays the RRS in the methanol solution. As expected, RRS are very similar to those in vacuum except for slight position shifts. For example, C=O stretching vibration of Aa decreases from 1669 cm^{-1} in vacuum to 1631 cm^{-1} in methanol solvent.

It is noted that the experiment[41] has only shown two remarkable peaks at 626 cm^{-1} and 1356 cm^{-1} for C343 in methanol solvent. Although both of them appear in the present simulated spectra (about 618 cm^{-1} and 1330 cm^{-1}), there are

still other strong peaks. Most of such peaks are associated with the vibration of –C=O, –OH, or –COOH. As is known that RRS are very sensitive to the polar solvent, and PCM model may not be enough to describe the interaction between C343 and methanol molecules. Further investigations with more reasonable solvent models, such as the cluster model, are needed to reveal the molecule-solvent interaction.

IV. CONCLUDING REMARKS

The vibrationally resolved spectral method and quantum chemical calculations, as well as the polarized continuum model, have been used to reveal the structural and spectral properties of Coumarin 343 (C343) isomers in vacuum and solution. In 12 different isomers, we have determined the most stable isomers in vacuum and methanol solution. It is found that the most stable syn-geometry with the intramolecular hydrogen bond (H-bond) in vacuum is switched into the anti geometry in solvent. The ionization potential of the anti conformer without H-bond is lower than the syn-conformer with H-bond, manifesting that the former may be easier to inject electrons to the conduction band of semiconductor than the latter. Compared to the gas phase, the presence of methanol solvent reduces the ionization potentials by about 1.6–1.8 eV, which may facilitate the electron injection. Further calculations for pure electronic absorption spectra reveal that C343 isomers and their deprotonated anions show redshift and blueshift, respectively, and all these spectra have a hyperchromic effect, compared to those in vacuum. From their vibrationally resolved spectra, we find that the 0-0 transitions in absorption and fluorescence are the strongest and only a single mode with low frequency (around 120 cm^{-1}) dominates the spectra. In addition, the modes with and without H-bond do not show explicitly different in the spectra. However, in the resonance Raman spectra, weak peaks appear in low frequencies and strong peaks in high frequencies, which is opposite to the absorption and emission. For the isomers with and without intramolecular hydrogen bond, their resonance Raman spectra also have explicit difference. These properties of the resonance Raman spectra can be used to identify the different isomers.

ACKNOWLEDGMENTS

This work is partially supported by the National Science Foundation of China (Grant Nos. 20833004, 21073146, and 21133007) and Research Fund for the Doctoral Program of Higher Education of China(Grant No. 200803840009).

[1]M. Grätzel, J. Photochem. Photobiol. C **4**, 145 (2003).
[2]A. Hagfeldt, G. Boschloo, L. Sun, L. Kloo, and H. Pettersson, Chem. Rev. **110**, 6595 (2010).
[3]J. N. Clifford, E. Martínez-Ferrero, A. Viterisi, and E. Palomares, Chem. Soc. Rev. **40**, 1635 (2011).
[4]G. A. Reynolds and K. H. Drexhage, Opt. Commun. **13**, 222 (1975).
[5]K. H. Drexhage, G. R. Erikson, G. H. Hawks, and G. A. Reynolds, Opt. Commun. **15**, 399 (1975).
[6]X. Allonas, J. P. Fouassier, M. Kaji, M. Miyasaka, and T. Hidaka, Polymer **42**, 7627 (2001).
[7]K. Hara *et al.*, J. Phys. Chem. B **107**, 597 (2003).
[8]X. Allonas, J.-P. Fouassier, H. Obeid, M. Kaji, and Y. Ichihashi, J. Photopolym. Sci. Technol. **1**, 35 (2004).
[9]Y. Harima *et al.*, Appl. Phys. Lett. **90**, 103517 (2007).
[10]A. Nattestad, M. Ferguson, R. Kerr, Y.-B. Cheng, and U. Bach, Nanotechnology **19**, 295304 (2008).
[11]A. Morandeira, G. Boschloo, A. Hagfeldt, and L. Hammarström, J. Phys. Chem. C **112**, 9530 (2008).
[12]K. Tominaga and G. C. Walker, J. Photochem. Photobiol., A **87**, 127 (1995).
[13]M. A. Kahlow, W. Jarzeba, T. J. Kang, and P. F. Barbara, J. Chem. Phys. **90**, 151 (1989).
[14]J. A. Gutierrez, R. D. Falcone, J. J. Silber, and N. M. Correa, J. Phys. Chem. A **114**, 7326 (2010).
[15]N. M. Correa and N. E. Levinger, J. Phys. Chem. B **110**, 13050 (2006).
[16]X. Zhou, J. W. Kaminski, and T. A. Wesolowski, Phys. Chem. Chem. Phys. **13**, 10565 (2011).
[17]F. Z. Badaoui and J. Bourson, Anal. Chim. Acta **302**, 341 (1995).
[18]J.-L. H. Jiwan, C. Branger, J.-P. Soumillion, and B. Valeur, J. Photochem. Photobiol., A **116**, 127 (1998).
[19]J. P. S. Farinha, P. Relógio, M.-T. Charreyre, T. J. V. Prazeres, and J. M. G. Martinho, Macromolecules **40**, 4680 (2007).
[20]T. Corrales, C. Abrusci, C. Peinado, and F. Catalina, Macromolecules **37**, 6596 (2004).
[21]A. E. Johnson, K. Tominaga, G. C. Walker, W. Jarzeba, and P. F. Barbara, Pure Appl. Chem. **65**, 1677 (1993).
[22]A. Mühlpfordt, R. Schanz, N. P. Ernsting, V. Farztdinov, and S. Gaimme, Phys. Chem. Chem. Phys. **1**, 3209 (1999).
[23]T. Honda, I. Fujii, N. Hirayama, N. Aoyama, and A. Miike, Acta Crystallogr. **C52**, 679 (1996).
[24]R. E. Riter, J. R. Kimmel, E. P. Undiks, and N. E. Levinger, J. Phys. Chem. B **101**, 8292 (1997).
[25]D. Pant and N. E. Levinger, Langmuir **16**, 10123 (2000).
[26]E. M. Corbeil and N. E. Levinger, Langmuir **19**, 7264 (2003).
[27]T. Yamasaki, O. Kajimoto, and K. Hara, J. Photochem. Photobiol., A **156**, 145 (2003).
[28]D. Pant, M. L. Guennec, B. Illien, and H. H. Girault, Phys. Chem. Chem. Phys. **6**, 3140 (2004).
[29]D. Pant and H. H. Girault, Phys. Chem. Chem. Phys. **7**, 3457 (2005).
[30]R. E. Riter, E. P. Undiks, and N. E. Levinger, J. Am. Chem. Soc. **120**, 6062 (1998).
[31]P. K. Singh, M. Kumbhakar, H. Pal, and S. Nath, J. Chem. Phys. **112**, 7771 (2008).
[32]R. J. Cave and J. E. W. Castner, J. Phys. Chem. A **206**, 12117 (2002).
[33]J. Preat, D. Jacquemin, and E. A. Perpète, Chem. Phys. Lett. **415**, 20 (2005).
[34]D. Jacquemin *et al.*, J. Chem. Phys. **125**, 164324 (2006).
[35]I. Kondov, H. Wang, and M. Thoss, Int. J. Quantum Chem. **106**, 1291 (2006).
[36]K. A. Nguyen, P. N. Day, and R. Pachter, J. Chem. Phys. **126**, 094303 (2007).
[37]Y. Kurashige, T. Nakajima, S. Kurashige, K. Hirao, and Y. Nishikitani, J. Phys. Chem. A **111**, 5544 (2007).
[38]X. Zhang, J. J. Zhang, and Y. Y. Xia, J. Photochem. Photobiol., A **194**, 167 (2008).
[39]B. M. Wong and J. G. Cordaro, J. Chem. Phys. **129**, 214703 (2008).
[40]T. Sakata, Y. Kawashima, and H. Nakano, Int. J. Quantum Chem. **109**, 1940 (2009).
[41]R. R. Frontiera, J. Dasgupta, and R. A. Mathies, J. Am. Chem. Soc. **131**, 15630 (2009).
[42]W. Zhao, Y. Ding, and Q. Xia, J. Comput. Chem. **32**, 545 (2011).
[43]R. S. de Armas, J. Oviedo, M. A. S. Miguel, and J. F. Sanz, J. Phys. Chem. C **115**, 11293 (2011).
[44]Y. J. Yan and S. Mukamel, J. Chem. Phys. **85**, 5908 (1986).
[45]F. Gao, W. Z. Liang, and Y. Zhao, Sci. China, Ser. B: Chem. **53**, 297 (2010).
[46]Y. Zhao and W. Z. Liang, J. Chem. Phys. **135**, 044108 (2011).
[47]W. Liang *et al.*, J. Chem. Phys. B **110**, 9908 (2006).
[48]Y. J. Yan and S. Mukamel, J. Chem. Phys. **86**, 6085 (1987).
[49]A. C. Albrecht, J. Chem. Phys. **34**, 1476 (1961).
[50]E. J. Heller, R. Sundberg, and D. Tannor, J. Phys. Chem. **86**, 1822 (1982).
[51]A. B. Myers, Chem. Rev. **96**, 911 (1996).
[52]A. B. Myers, Acc. Chem. Res. **30**, 519 (1997).
[53]A. M. Kelly, J. Phys. Chem. A **103**, 6891 (1999).
[54]C. Lee, W. Yang, and R. G. Parr, Phys. Rev. B **37**, 785 (1988).
[55]B. Miehlich, A. Savin, H. Stoll, and H. Preuss, Chem. Phys. Lett. **157**, 200 (1989).

[56]A. D. Becke, J. Chem. Phys. **98**, 5648 (1993).
[57]R. Bauernschmitt and R. Ahlrichs, Chem. Phys. Lett. **256**, 454 (1996).
[58]M. E. Casida, C. Jamorski, K. C. Casida, and D. R. Salahub, J. Chem. Phys. **108**, 4439 (1998).
[59]R. E. Stratmann, G. E. Scuseria, and M. J. Frisch, J. Chem. Phys. **109**, 8218 (1998).
[60]C. V. Caillie and R. D. Amos, Chem. Phys. Lett. **308**, 249 (1999).
[61]C. V. Caillie and R. D. Amos, Chem. Phys. Lett. **317**, 159 (2000).
[62]F. Furche and R. Ahlrichs, J. Chem. Phys. **117**, 7433 (2002).
[63]G. Scalmani *et al.*, J. Chem. Phys. **124**, 094107 (2006).
[64]V. Barone and M. Cossi, J. Phys. Chem. A **102**, 1995 (1998).
[65]M. Cossi, N. Rega, G. Scalmani, and V. Barone, J. Comput. Chem. **24**, 669 (2003).
[66]See http://cccbdb.nist.gov/vsf.asp for vibrational frequency scaling factors for diffeernt functionals and different basis sets.
[67]M. J. Frisch, G. W. Trucks, H. B. Schlegel *et al.*, GAUSSIAN 09, Revision B.01, Gaussian, Inc., Wallingford, CT, 2010.
[68]See supplementary material at http://dx.doi.org/10.1063/1.3693264 for pure electronic absorption spectra, vibrational resolved electronic absorption and fluorescence spectra, resonance Raman spectra, normal mode shifts, and the assignments of spectra peaks in the simulated spectra .
[69]R. Huber, J. E. Moser, M. Grätzel, and J. Wachtveitl, Chem. Phys. **285**, 39 (2002).
[70]A. Warshel and P. Dauber, J. Chem. Phys. **66**, 5477 (1977).
[71]R. A. Harris, R. Mathies, and A. Myers, Chem. Phys. Lett. **94**, 327 (1983).